Radiology

ORIGINAL RESEARCH • COMPUTER APPLICATIONS

A CT-based Radiomics Signature Is Associated with Response to Immune Checkpoint Inhibitors in Advanced Solid Tumors

Marta Ligero, MSc • Alonso Garcia-Ruiz, MSc • Cristina Viaplana, MSc • Guillermo Villacampa, MSc • Maria V. Raciti, MD • Jaid Landa, MD • Ignacio Matos, MD • Juan Martin-Liberal, MD, PhD • Maria Ochoa-de-Olza, MD • Cinta Hierro, MD • Joaquin Mateo, MD, PhD • Macarena Gonzalez, MD • Rafael Morales-Barrera, MD • Cristina Suarez, MD • Jordi Rodon, MD, PhD • Elena Elez, MD, PhD • Irene Braña, MD, PhD • Eva Muñoz-Couselo, MD • Ana Oaknin, MD • Roberta Fasani, MD • Paolo Nuciforo, MD, PhD • Debora Gil, PhD • Carlota Rubio-Perez, PhD • Joan Seoane, PhD • Enriqueta Felip, MD, PhD • Manuel Escobar, MD • Josep Tabernero, MD, PhD • Joan Carles, MD • Rodrigo Dienstmann, MD • Elena Garralda, MD • Raquel Perez-Lopez, MD, PhD

From the Radiomics Group, Vall d'Hebron Institute of Oncology (VHIO), Cellex Center, Natzaret 115-117, Barcelona 08035, Spain (M.L., A.G.R., R.P.L.); Oncology Data Science (ODysSey) Group, Vall d'Hebron Institute of Oncology (VHIO), Barcelona, Spain (C.V., G.V., R.D.); Institute of Radiology, Foundation IRCCS Polyclinic San Matteo, Pavia, Italy (M.V.R.); Department of Radiology, Bellvitge University Hospital, L'Hospitalet de Llobregat, Spain (J.L.); Department of Medical Oncology, Vall d'Hebron University Hospital and Institute of Oncology (VHIO), Barcelona, Spain (I.M., J.M.L., M.O.d.O., C.H., J.M., M.G., R.M.B., C.S., J.R., E.E., I.B., E.M.C., A.O., E.F., J.T., J.C., E.G.); Department of Molecular Oncology, Vall d'Hebron Institute of Oncology (VHIO), Barcelona, Spain (R.F., P.N.); Computer Vision Center, Department of Computer Science, Autonomous University of Barcelona, Cerdanyola del Vallès, Spain (D.G.); Vall d'Hebron Institute of Oncology (VHIO), Vall d'Hebron University Hospital (HUVH), Autonomous University of Barcelona, Institució Catalana de Recerca i Estudis Avançats (ICREA) and CIBERONC, Barcelona, Spain (C.R.P., J.S.); Department of Radiology, Vall d'Hebron University Hospital, Barcelona, Spain (M.E., R.P.L.); and Department of Medicine, Autonomous University of Barcelona (UAB), Barcelona, Spain (J.T.). Received March 9, 2020; revision requested April 6; revision received November 2; accepted November 11. **Address correspondence to** R.P.L. (e-mail: *rperez@vhio.net*).

Study supported by the Banco Bilbao Vizcaya Argentaria, Fundació La Caixa (RTI2018-095209-B-C21, FIS-G64384969), Generalitat de Catalunya (2017-SGR-1624), and CERCA-Programme. J.M. and R.P.L. supported by Prostate Cancer Foundation Young Investigator Awards. R.P.L. supported by a CRIS Foundation Talent Award (TALENT19-05) and the Instituto de Salud Carlos III-Investigación en Salud (PI18/01395). D.G. is supported by Serra Hunter Fellowship.

Conflicts of interest are listed at the end of this article.

See also the editorial by Summers in this issue.

Radiology 2021; 00:1–11 • https://doi.org/10.1148/radiol.2021200928 • Content codes: IN CT

Background: Reliable predictive imaging markers of response to immune checkpoint inhibitors are needed.

Purpose: To develop and validate a pretreatment CT-based radiomics signature to predict response to immune checkpoint inhibitors in advanced solid tumors.

Materials and Methods: In this retrospective study, a radiomics signature was developed in patients with advanced solid tumors (including breast, cervix, gastrointestinal) treated with anti–programmed cell death–1 or programmed cell death ligand–1 monotherapy from August 2012 to May 2018 (cohort 1). This was tested in patients with bladder and lung cancer (cohorts 2 and 3). Radiomics variables were extracted from all metastases delineated at pretreatment CT and selected by using an elastic-net model. A regression model combined radiomics and clinical variables with response as the end point. Biologic validation of the radiomics score with RNA profiling of cytotoxic cells (cohort 4) was assessed with Mann-Whitney analysis.

Results: The radiomics signature was developed in 85 patients (cohort 1: mean age, 58 years ± 13 [standard deviation]; 43 men) and tested on 46 patients (cohort 2: mean age, 70 years ± 12; 37 men) and 47 patients (cohort 3: mean age, 64 years ± 11; 40 men). Biologic validation was performed in a further cohort of 20 patients (cohort 4: mean age, 60 years ± 13; 14 men). The radiomics signature was associated with clinical response to immune checkpoint inhibitors (area under the curve [AUC], 0.70; 95% CI: 0.64, 0.77; $P < .001$). In cohorts 2 and 3, the AUC was 0.67 (95% CI: 0.58, 0.76) and 0.67 (95% CI: 0.56, 0.77; $P < .001$), respectively. A radiomics-clinical signature (including baseline albumin level and lymphocyte count) improved on radiomics-only performance (AUC, 0.74 [95% CI: 0.63, 0.84; $P < .001$]; Akaike information criterion, 107.00 and 109.90, respectively).

Conclusion: A pretreatment CT-based radiomics signature is associated with response to immune checkpoint inhibitors, likely reflecting the tumor immunophenotype.

Online supplemental material is available for this article.

Cancer immunotherapy is one of the most promising anticancer treatment strategies. The landmark example of immunotherapy success was the development of immune checkpoint inhibitors (programmed cell death–1 [PD-1] and programmed cell death ligand–1 [PD-L1]). Several monoclonal anti–PD-1 and anti–PD-L1 antibodies, such as pembrolizumab, nivolumab, and atezolizumab, are now approved for the treatment of different tumor types, including urinary tract and lung cancer (1–10). Despite the excellent results of immune checkpoint inhibitor trials, some caveats remain about optimal patient stratification (11,12). Although some

Abbreviations

AUC = area under the curve, PD-1 = programmed cell death protein–1, PD-L1 = programmed cell death protein ligand–1, RECIST = Response Evaluation Criteria in Solid Tumors

Summary

A CT-based radiomics signature, based on histogram, shape, and local-regional texture features, showed an association with immune response in advanced solid tumors.

Key Results

- In this retrospective study of 85 patients, a CT-based 14-feature radiomics signature (histogram, shape, and local-regional texture) was associated with response to immune checkpoint inhibitors in advanced solid tumors (area under curve [AUC], 0.70; $P < .001$; sensitivity, 75%; specificity, 53%).
- Radiomics combined with clinical data (baseline albumin and lymphocytes) improved response classification performance compared with radiomics or clinical data alone (AUC, 0.74 vs 0.70 and 0.64, respectively).

patients achieve dramatic responses, others do not respond at all. In addition, immune checkpoint inhibitors can cause serious side effects in some patients (13).

Further immunotherapy agents are being tested in combination with PD-1/PD-L1 inhibitors to improve the response of immunotherapy-sensitive tumors and to convert immunotherapy-insensitive tumors into responsive tumors (14). Given this, it is critical to optimally identify patients more likely to respond to immune checkpoint inhibitors to maximize patient benefit, minimize risks, and accelerate drug development. Currently, tumor PD-L1 expression, microsatellite instability status, and tumor mutational burden are imperfect predictive biomarkers of response to anti–PD-1/PD-L1 antibodies, with varying performance across different tumor types (15,16).

Radiomics derives quantitative variables from imaging data of tumor tissues by the application of data mining algorithms to medical images (17–21). Much of the discussion about personalized medicine has focused on molecular characterization by using genomic and proteomic technologies. However, these often require biopsies or invasive operations to extract and analyze small portions of tumor tissue, which do not allow for complete tumor characterization. Tumors are spatially and temporally heterogeneous (22,23), giving imaging an advantage in guiding personalized treatment because it yields a comprehensive view of the entire tumor. Radiomics can provide noninvasive tools to study tumor biology, capture tumor heterogeneity, and monitor tumor evolution and response to therapy.

In this study, we aimed to develop and test a radiomics signature from baseline (pretreatment) CT scans to predict response to anti–PD-1/PD-L1 in patients with advanced solid tumors. For a biologic validation of this radiomics signature, associations with tumor-infiltrating lymphocytes and RNA profiling of cytotoxic cells were performed. We also explored the integration of CT-based radiomics and clinical data into a multidimensional signature for response.

Materials and Methods

The institutional review board approved this retrospective study. All patients included in the clinical trials provided written informed consent. Need for informed consent for the computational analysis of the images was waived. Clinical trials included in the study are listed in Table E1 (online).

Study Sample

Cohort 1 (training set) included patients treated with anti–PD-1/PD-L1 monotherapy in phase I clinical trials from August 2012 to May 2018. Cohort 2 (test set 1) was composed of patients with bladder cancer treated with anti–PD-1/PD-L1 from June 2013 to May 2018. Cohort 3 (test set 2) was composed of patients with lung cancer treated with anti–PD-1/PD-L1 from December 2013 to April 2016. Cohort 4 (biologic validation set) was

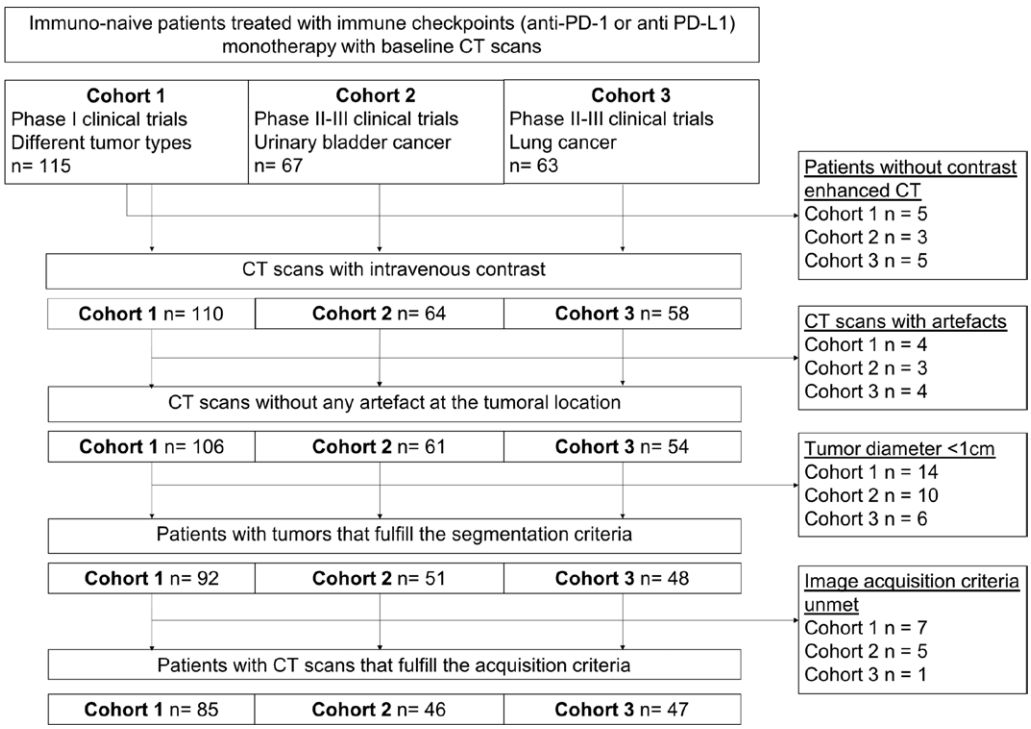

Figure 1: Flowchart shows inclusion/exclusion for all three patient cohorts. PD-1 = programmed cell death protein–1, PD-L1 = programmed cell death protein ligand–1.

composed of patients with different tumor types and gene expression profiling from solid tumor biopsy samples where contrast-enhanced CT was performed within 4 months before biopsy. None of these patients had been included in cohorts 1, 2, or 3. All patients were treated at the Vall d'Hebron Institute of Oncology (Barcelona, Spain).

Exclusion criteria for this study comprised patients who had received previous immunotherapies, nonenhanced CT, CT with artifacts, nonmeasurable lesions per Response Evaluation Criteria in Solid Tumors (RECIST) 1.1, and lesions with cystic changes or cavitation. We also excluded patients in whom the biopsy had been performed before the CT to avoid biopsy-related changes. The study flowchart is shown in Figure 1.

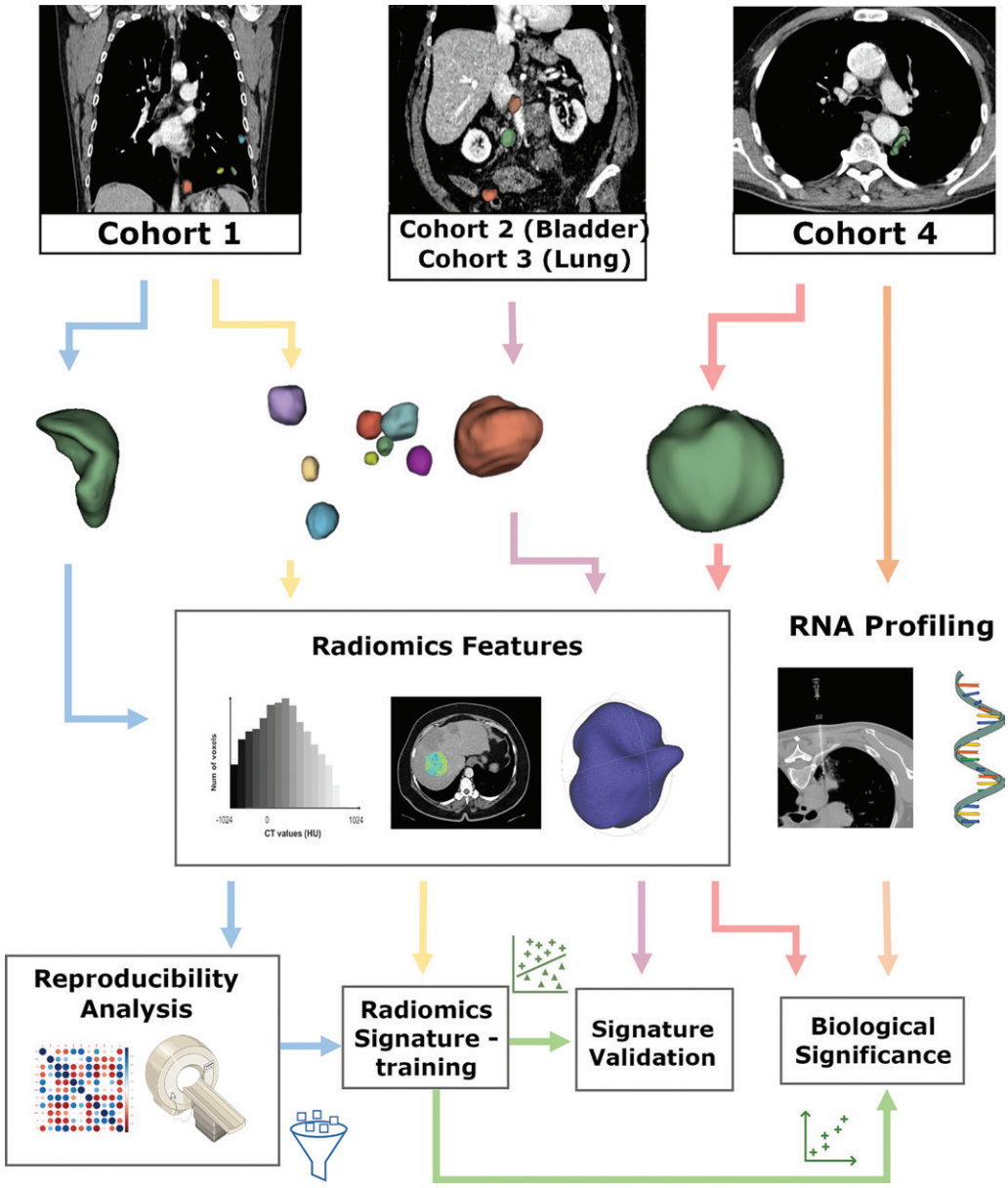

Figure 2: Schema shows radiomics workflow. The model was trained in cohort 1. Features were selected according to the reproducibility analysis. Then, the signature was tested in cohorts 2 and 3. Finally, a biologic validation was implemented by using RNA profiling in cohort 4.

Image Data Acquisition and Analysis

CT scans obtained within 28 days before the treatment start date were analyzed. Contrast-enhanced CT scans were acquired by using 16- or 64-channel CT scanners (Siemens, Philips, and GE Healthcare) in the axial plane with tube voltage of 100–130 kV, section thickness of 2–5 mm, and section interval of 1.25–5 mm (Table E2 [online]). All well-defined lesions per patient were delineated by a radiologist (R.P.L., with 10 years of experience in oncologic imaging), blinded to the clinical outcome, by using the 3DSlicer version 4.8.1 (24) semiautomatic contouring tool.

Images were resampled to isometric voxels of $1 \times 1 \times 1$ mm^3 by using spline interpolation. Hounsfield units were binarized to discrete values of 10 HU (25). CT-based radiomics features (first order, shape, and texture) were derived by using the Pyradiomics package (version 2.2.0) for Python (version 3.7.1), compliant with the Image Biomarker Standardization Initiative guidelines (26,27) (Table E3 [online]). Radiomics data were standardized to zero-centered distributions with logarithmic transformations.

Clinical Data

Clinical and laboratory data were collected from electronic patient records. These included age, sex, tumor type, Eastern Cooperative Oncology Group performance status, number of organs with metastasis, lactate dehydrogenase level, leukocyte count, albumin level, lymphocyte count, platelet count, and neutrophil count at baseline. Outcome data included clinical benefit and overall survival. Clinical benefit was defined as stable disease after 5 months of treatment or partial or complete response within the first 5 months of treatment according to RECIST 1.1 (28,29).

Table 1: Study Sample Characteristics

Parameter	Cohort 1 (n = 85)	Cohort 2 (n = 46)	Cohort 3 (n = 47)	Cohort 4 (n = 20)
Mean age (y)*†	58 ± 13 (29–85)	70 ± 12 (44–91)	64 ± 11 (39–88)	60 ± 14 (25–85)
Sex				
Female	42 (49)	9 (20)	7 (15)	6 (30)
Male	43 (51)	37 (80)	40 (85)	14 (70)
Primary tumor type				
Breast	14 (16)	…	…	…
Cervix	10 (12)	…	…	…
Other	10 (12)	…	…	1 (5)
Gastrointestinal	9 (11)	…	…	…
Melanoma	8 (9)	…	…	1 (5)
Thyroid	6 (7)	…	…	…
Lung	6 (7)	…	47 (100)	15 (75)
Bladder	6 (7)	46 (100)	…	…
Head and neck	5 (6)	…	…	…
Ovary	3 (4)	…	…	3 (15)
Pleura	2 (2)	…	…	…
Thymus	2 (2)	…	…	…
Kidney	2 (2)	…	…	…
Adrenal	2 (2)	…	…	…
Treatment‡				
PD-1 immune checkpoint inhibitor	38 (45)	21 (46)	35 (75)	…
PD-L1 immune checkpoint inhibitor	47 (55)	25 (54)	12 (25)	…
Best response				
Complete response	5 (6)	7 (15)	2 (4)	…
Partial response	7 (8)	15 (33)	11 (24)	…
Stable disease	41 (48)	6 (13)	17 (36)	…
Progressive disease	32 (38)	18 (39)	17 (36)	…
Lesion location				
Node	86 (36)	66 (47)	46 (44)	4 (20)
Liver	53 (22)	30 (21)	22 (21)	1 (5)
Lung	60 (25)	28 (20)	26 (25)	11 (55)
Other	37 (16)	16 (12)	10 (10)	4 (20)
No. of lesions	236	140	104	20
Mean lesion size (mm)*	35 (10–139)	35 (10–259)	39 (13–96)	40 (14–99)
Mean no. of lesions per patient*	2.77 (1–17)	3.04 (1–11)	2.21 (1–10)	1

Note.—Data in parentheses are percentages unless otherwise indicated. Cohort 1 is training, cohort 2 is bladder test set, cohort 3 is lung test set, and cohort 4 is biologic validation. PD-1 = programmed cell death protein–1, PD-L1 = programmed cell death protein ligand–1.

*Data in parentheses are range.

†Data are ± standard deviation.

‡Atezolizumab, avelumab, durvalumab, retifanlimab, pembrolizumab, nivolumab, cemiplimab, PDR001, FAZ053.

Patient follow-up was considered as the time between treatment baseline (treatment start date) and discontinuation.

Exploring Biologic Significance of CT-based Radiomics Signature

Assessment and immunophenotyping of tumor-infiltrating lymphocytes by NanoString (NanoString Technologies) gene expression profiling of tumor samples were performed at the Vall d'Hebron Institute of Oncology (30). The CT-based radiomics score and the enrichment score of cytotoxic cells were calculated from the same biopsied lesion. The enrichment score was computed as the mean of the log-2 z-score of the transformed expression values of the gene set, after background thresholding and housekeeping adjustment. The cytotoxic cell gene set included *CD8A*, *GZMA*, *GZMB*, and *PRF1* genes. Methods for assessment of tumor-infiltrating lymphocytes and radiomics–tumor-infiltrating lymphocyte associations are described in Appendix E1 (online).

Statistical Analysis

Test-retest reproducibility based on the acquisition protocols and interobserver reproducibility were assessed by using intraclass correlation coefficients (31) (Appendix E1 [online]). An elastic-net model was implemented for feature selection in both radiomics and clinical-radiomics signature. The regularization parameters λ and α were determined by using cross validation.

Table 2: CT-based Radiomics Signature and Radiomics-Clinical Signature, Variables, and Coefficients

Variable	β Model Coefficient
CT-based radiomics signature	
First-order entropy	11.73 (−4.14, 27.6)
First-order total energy	4.18 (−0.78, 9.13)
First-order uniformity	5.56 (−4.11, 15.22)
GLCM inverse difference moment	−4.66 (−18.37, 9.06)
GLCM joint entropy	−4.67 (−14.18, 4.84)
GLDM dependence nonuniformity normalized	−9.24 (−21.23, 2.75)
GLDM dependence variance	−6.9 (−15.62, 1.81)
GLDM large dependence emphasis	3.82 (−6.1, 13.73)
Elongation	0.54 (−9.04, 10.13)
Least axis length*	0.62 (−7.55, 8.78)
Major axis length*	3.16 (−23.96, 30.29)
Maximum 2D diameter column	0.4 (−5.76, 6.56)
Minor axis length*	−7.53 (−35.08, 20.01)
Surface area	−1.66 (−26.27, 22.95)
Liver	−1.77 (−7.21, 3.67)
Other	5.33 (−1.38, 12.05)
CT-based radiomics and clinical signature	
Mean radiomics score	2.06 (0.64, 3.48)
Baseline lymphocytes (× 10^9/L)	0.49 (−0.16, 1.14)
Baseline albumin level (g/dL)	0.39 (−0.1, 0.88)

Note.—Data in parentheses are 95% CIs. GLCM = gray level co-occurrence matrix, GLDM = gray level dependence matrix, 2D = two-dimensional.

*Major axis length defined as the largest axis length of the region-of-interest–enclosing ellipsoid; minor axis length defined as the second-largest axis length of the region-of-interest–enclosing ellipsoid; least axis length defined as the smallest axis length of the region-of-interest–enclosing ellipsoid.

The radiomics signature was implemented by using generalized linear mixed models, including robust radiomics features (defined as intraclass correlation coefficient ≥ 0.7) selected by elastic net, lesion location (node, liver, lung, and others) and with consideration of patient identification as a random effect to adjust for the intrapatient variability for lesions from the same patient. The end point of the model was clinical benefit.

The clinical-radiomics signature was developed by using generalized linear models that included mean radiomics score per patient and clinical data with clinical benefit as the end point. The mean radiomics score per patient was derived from the probability (p) defined as follows:

$$\ln\left(\frac{p}{1-p}\right) = X\beta + Zu \quad (1),$$

$$Radscore_{pat} = \sum_{i=1}^{N_{lesions}} \frac{Radscore_i}{N_{lesions}} \quad (2),$$

where X is a matrix of $N_{pat}xp$ of p predictor variables, N_{pat} is number of patients, and β is a $px1$ vector of the fixed-effects coefficients. Z is the $N_{pat}xq$ matrix for q random effects, and u is a $qx1$ vector of the random-effect coefficients. The radiomics score per patient ($Radscore_{pat}$) is the average of all the lesion radiomics scores in a patient as defined in Equation (2) where $N_{lesions}$ is the number of lesions and $Radscore_i$ is the radiomic score per lesion.

The area under the curve (AUC) and 95% CI (DeLong method) were determined from the receiver operating characteristic curve, and the P value was assessed by using the Mann-Whitney U test. The decision threshold to determine the sensitivity and specificity was defined by maximizing the sensitivity given a minimal value of specificity of 50%.

The model performances obtained by using radiomics predictive score only and by combining radiomics score with clinical data were compared by using Akaike information criterion. Hosmer-Lemeshow goodness-of-fit test was reported as the calibration statistic. The radiomics signature was internally validated with a stratified 10-fold cross-validation analysis (Appendix E1 [online]).

A patient-level analysis was performed by using logistic regression to obtain odds ratios.

A Cox proportional hazard regression model was used to associate overall survival with the radiomics and radiomics-clinical score. The proportionality of hazard assumptions was assessed with Schoenfeld residuals. Univariate and multivariate analyses were performed for each variable from the radiomics-clinical signature. Overall survival analysis was performed by using the Kaplan–Meier method after score dichotomization. Patients who did not reach the end point were censored to the last follow-up date. The Harrell C-index was assessed to compare both scoring systems.

Associations between radiomics score with tumor-infiltrating lymphocytes and cytotoxic immunophenotype enrichment were evaluated by using Mann-Whitney analysis. The P value α level was considered to indicate significance at .05.

Statistical analyses were performed by using R software, version 3.5.0. The R packages used are listed in Table E4 (online). The code can be found at *https://github.com/mligerhe/Immuno-CTrad*. The study workflow is summarized in Figure 2.

Results

Study Patient Characteristics

Of 115 patients from cohort 1, 67 patients from cohort 2, and 63 patients from cohort 3, we excluded 13 because of noncontrast CT scans, 11 because of artifacts at the tumor site, 30 without measurable lesions per RECIST 1.1, and 13 whose scans did not fulfill the image acquisition criteria (Fig 1).

In cohort 1, a total of 236 lesions (mean number of lesions per patient, three; range, one to 17 lesions per patient) from the 85 patients (mean age, 58 years ± 13 [standard deviation]; 42 women [mean age, 55 years ± 12] and 43 men [mean age, 62 years ± 13]) were included in the final analysis. The median follow-up period was 4 months (interquartile range, 2–12 months); 51% (43 of 85) of the patients showed a clinical benefit and 49% (42 of 85) of the patients did not show a complete response, partial response, or stable disease after 5 months of treatment.

In cohort 2, a total of 140 lesions (mean number of lesions per patient, three; range, one to 11 lesions per patient) from the 46 patients (mean age, 70 years ± 12; nine women [mean age, 70 years ± 9] and 37 men [mean age, 70 years ± 12]) were included in the final analysis. The median follow-up time was 4 months (interquartile range, 2–10 months); 54% (25 of 46) of the patients showed a clinical benefit, and 46% (21 of 46) did not.

In cohort 3, a total of 104 lesions (mean number of lesions per patient, two; range, one to 10 lesions per patient) from the 47 patients (mean age, 64 years ± 11; seven women [mean age, 55 years ± 6] and 40 men [mean age, 66 years ± 11]) were included in the final analysis. The median follow-up time was 5 months (interquartile range, 2–10 months);

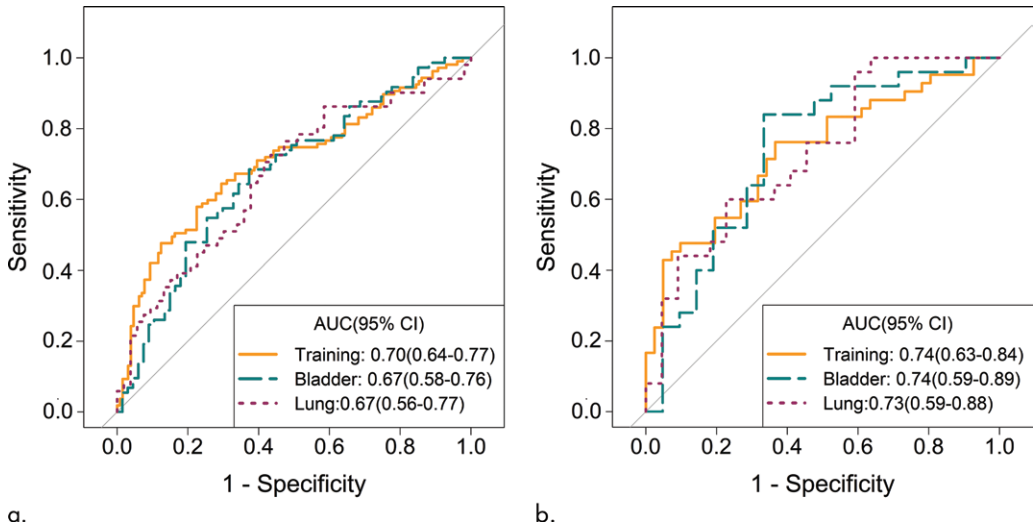

Figure 3: Receiver operating characteristic curves of **(a)** radiomics and **(b)** radiomics-clinical signature for predicting response to immune checkpoint inhibitors in cohort 1 (training set), cohort 2 (bladder test set), and cohort 3 (lung test set). AUC = area under the curve.

Table 3: Radiomics, Radiomics-Clinical, and Clinical-only Signature Performance

Cohort	AUC	*P* Value	Sensitivity (%)	Specificity (%)	NPV (%)	PPV (%)	Positive LR	Negative LR
Radiomics signature*								
Cohort 1	0.70 [0.64, 0.77]	<.001	75 (80/107) [65, 83]	53 (68/129) [44, 62]	72 (68/95) [61, 80]	57 (80/141) [48, 65]	1.58 [1.28, 1.96]	0.48 [0.33, 0.69]
Cohort 2	0.67 [0.58, 0.76]	<.001	73 (53/73) [61, 82]	55 (37/67) [43, 67]	65 (37/57) [51, 77]	64 (53/83) [53, 74]	1.62 [1.2, 2.19]	0.5 [0.32, 0.76]
Cohort 3	0.67 [0.56, 0.77]	<.001	73 (37/51) [58, 84]	57 (30/53) [42, 70]	68 (30/44) [52, 81]	62 (37/60) [48, 74]	1.67 [1.18, 2.37]	0.48 [0.29, 0.8]
Radiomics-clinical signature†								
Cohort 1	0.74 [0.63, 0.84]	<.001	77 (33/43) [61, 88]	59 (25/42) [42, 74]	71 (25/35) [53, 85]	66 (33/50) [50, 78]	1.87 [1.23, 2.74]	0.38 [0.22, 0.74]
Cohort 2	0.74 [0.59, 0.89]	<.001	84 (21/25) [64, 95]	67 (14/21) [43, 85]	78 (14/18) [52, 94]	75 (21/28) [55, 89]	2.52 [1.34, 4.72]	0.24 [0.09, 0.62]
Cohort 3	0.73 [0.59, 0.88]	<.001	68 (17/25) [46, 85]	55 (12/22) [32, 76]	60 (12/20) [36, 81]	63 (17/27) [42, 81]	1.5 [0.88, 2.54]	0.59 [0.3, 1.17]
Clinical signature‡								
Cohort 1	0.64 [0.52, 0.76]	.01	70 (30/43) [53, 82]	55 (23/42) [37, 69]	66 (23/35) [45, 79]	61 (30/49) [45, 74]	1.50 [1.01, 2.19]	0.55 [0.34, 0.98]
Cohort 2	0.67 [0.5, 0.84]	.02	84 (21/25) [64, 95]	48 (10/21) [26, 70]	71 (10/14) [42, 92]	66 (21/32) [47, 81]	1.6 [1.03, 2.5]	0.34 [0.12, 0.92]
Cohort 3	0.65 [0.49, 0.81]	.04	76 (19/25) [55, 91]	50 (11/22) [28, 72]	65 (11/17) [38, 86]	63 (19/30) [44, 80]	1.52 [0.95, 2.44]	0.48 [0.21, 1.08]

Note.—Data in parentheses are numerator/denominator; data in brackets are 95% CIs. LR = likelihood ratio, NPV = negative predictive value, PPV = positive predictive value.

*Radiomics signature including 14 variables from histogram, shape, and local-regional texture.

†Radiomics-clinical signature including mean radiomics score per patient, albumin level, and lymphocyte count.

‡Clinical signature including albumin level and lymphocyte counts.

53% (25 of 47) of the patients showed a clinical benefit, and 47% (22 of 47) did not.

In cohort 4, 20 patients (mean age, 60 years ± 13; six women [mean age, 55 years ± 9] and 14 men [mean age, 63 years ± 15]) were included in the final analysis for biologic validation. One lesion per patient was delineated, corresponding to the biopsied tumor in which the RNA profiling was performed. The study sample characteristics are summarized in Table 1.

Predictive Model Development and Testing

Twenty-six radiomics features showed an intraclass correlation coefficient of 0.7 or greater in the reproducibility analysis (Appendix E1, Table E5 [online]). Elastic-net parameters were set to λ of 0.001 and α of 1 for the radiomics signature, and 14 from 26 variables were retained (Table 2).

In terms of classification performance, the training set had an AUC of 0.70 (95% CI: 0.64, 0.77; $P < .001$), the bladder test set had an AUC of 0.67 (95% CI: 0.58, 0.76; $P < .001$), and the lung test set had an AUC of 0.67 (95% CI: 0.56, 0.77; $P < .001$) (Fig 3a). Sensitivity, specificity, negative predictive value, and positive predictive value for identifying patients with clinical benefit with an optimal cutoff of 0.29 are summarized in Table 3. The radiomics signature showed no evidence of poor fit (Hosmer-Lemeshow, $P > .05$).

Integrating Radiomics and Clinical Data

The radiomics-clinical elastic-net feature selection retained with nonzero coefficients (elastic-net to λ = 0.08, α = .9) the mean radiomics score per patient and two clinical features (albumin and lymphocytes; Table 2).

The radiomics-clinical model showed an AUC of 0.74 (95% CI: 0.63, 0.84; $P < .001$) in the training set and AUCs of 0.74 (95% CI: 0.59, 0.89; $P < .001$) and 0.73 (95% CI: 0.59, 0.88; $P = .002$) for predicting clinical benefit in cohorts 2 and 3, respectively. Sensitivity, specificity, negative predictive value, and positive predictive value for identifying patients with clinical benefit with an optimal cutoff of 0.45 are summarized in Table 3. The radiomics-clinical model showed no evidence of poor fit (Hosmer-Lemeshow, $P > .05$). The radiomics-clinical signature presented a better performance compared with the radiomics-only signature (Akaike information criterion, 107.00 and 109.90, respectively).

Clinical signature performance is reported in Table 3 and Figure E1 (online).

In the patient-level analysis, an increase in the mean score per patient was associated with clinical benefit in all cohorts (cohort 1: odds ratio, 1.22 [95% CI: 1.07, 1.41], $P = .004$; cohort 2: odds ratio, 1.34 [95% CI: 1.10, 1.70], $P = .007$; cohort 3: odds ratio, 1.22 [95% CI: 1.03, 1.47], $P = .02$) (Fig 4).

The radiomics-clinical score was associated with overall survival in all cohorts (cohort 1: hazard ratio, 0.14 [95% CI: 0.04, 0.51], $P = .003$; cohort 2: hazard ratio, 0.02 [95% CI: 0.00, 0.20], $P = .001$; cohort 3: hazard ratio, 0.13 [95% CI: 0.03, 0.57], $P = .01$) (Table 4). Univariate and multivariate Cox proportional hazard ratios are in Table E6 (online).

Patients with a high radiomics-clinical score (score > 0.45) showed improved overall survival compared with those with a low radiomics-clinical score (score ≤ 0.45); the 24-month overall survival in cohort 2 was 53% (95% CI: 35, 79) versus 25% (95% CI: 10, 62; $P = .002$), and in cohort 3 it was 36% (95% CI: 21, 60) versus 5% (95% CI: 1, 34; $P = .02$) (Fig 5).

Exploring the Biologic Significance of the CT-based Radiomics Signature

Tumor RNA profiling through NanoString and CT scans was available for 20 patients (cohort 4) (sample characteristics are

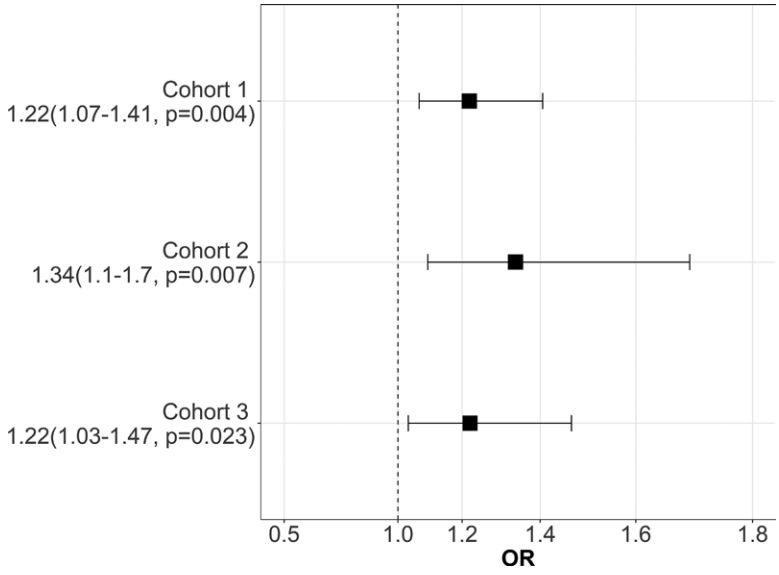

Figure 4: Association of the mean radiomics score per patient with clinical benefit for patient-level analysis in cohort 1 (phase I training set), cohort 2 (bladder test set), and cohort 3 (lung test set). Data in parentheses are 95% CIs. OR = odds ratio.

Table 4: Hazard Ratio and C-index for Association of Mean Radiomics and Radiomics-Clinical Score per Patient with Overall Survival in Cohorts 1, 2, and 3

Variable	Hazard Ratio	*P* Value	C-index
Radiomics score			
Cohort 1	0.56 (0.28, 1.14)	.11	0.61 (0.52, 0.7)
Cohort 2	0.11 (0.03, 0.37)	<.001	0.74 (0.65, 0.82)
Cohort 3	0.38 (0.16, 0.88)	.03	0.61 (0.51, 0.7)
Radiomics-clinical score			
Cohort 1	0.14 (0.04, 0.51)	.003	0.65 (0.56, 0.73)
Cohort 2	0.02 (0, 0.2)	.001	0.72 (0.62, 0.82)
Cohort 3	0.13 (0.03, 0.57)	.01	0.65 (0.57, 0.73)

Note.—Data in parentheses are 95% CIs.

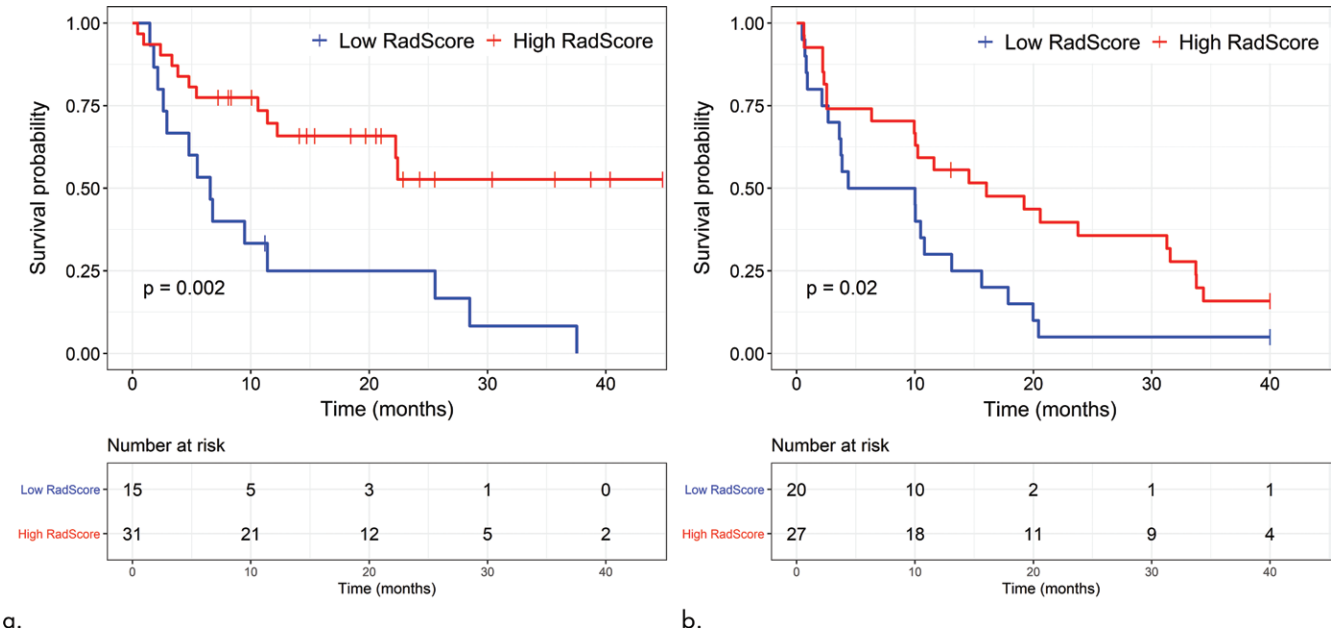

a. b.

Figure 5: Kaplan-Meier overall survival curve analysis in the cohort 2 (**a**) and cohort 3 (**b**) test sets. The CT-based radiomics and clinical score was defined as high (>0.45) or low (≤0.45), according to the receiver operating characteristic cutoff maximizing sensitivity. RadScore = radiomics score.

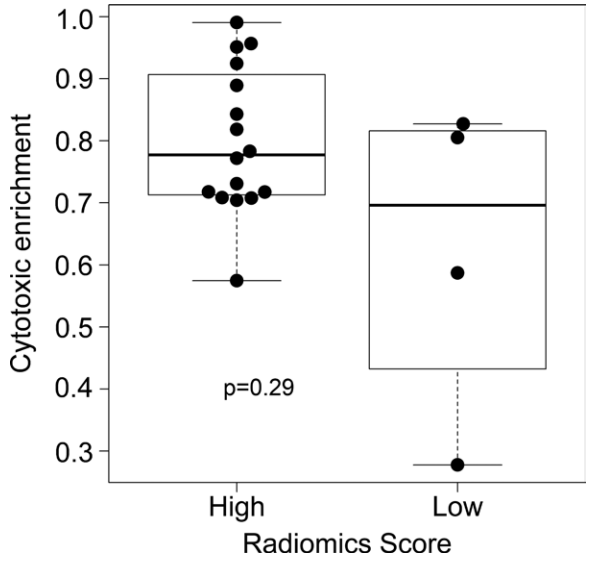

Figure 6: Association between cytotoxic immunophenotype enrichment score and the CT-based radiomics score in cohort 4. The CT-based radiomics score was defined as high (>0.29) or low (≤0.29), according to the receiver operating characteristic cutoff maximizing sensitivity. Dots correspond to the Cytotoxic enrichment value of each patient's lesion and whiskers corresponds to the minimum and maximum values of each radiomics score group.

in Table 1). In this cohort, tumors with a high radiomics score (>0.29 according to the cutoff point of the receiver operating characteristic curve) showed higher values of immune cytotoxic cells compared with the tumors with low radiomics score, but this difference was not significant (0.80 ± 0.12 vs 0.62 ± 0.25; P = 0.29) (Fig 6).

Tumor samples for tumor-infiltrating lymphocyte quantification were available from 75 patients in cohorts 1 and 2 (Table E7 [online]). No association was identified between tumor-infiltrating lymphocytes and high versus low mean radiomics score (score, >0.29 or ≤0.29) (mean, 2.37 ± 1.12 vs 1.89 ± 1.19; P = .36) (Appendix E1, Fig E2 [online]).

Discussion

Although immune checkpoint inhibitors have transformed the management of many tumor types, response rates are still suboptimal, and better treatment selection is required. In this study, we developed a radiomics signature that potentially allows stratification of patients who are more likely to benefit from immune checkpoint inhibitors, achieving a 75% sensitivity and 53% specificity. The radiomics signature consisted of 14 features related to first-order histogram, shape, and local-regional texture (gray level–dependent matrix and gray level co-occurrence matrix derived). The negative coefficient of gray level–dependent matrix dependence variance and dependence nonuniformity normalized features, indicating homogeneous tumors, were associated with a higher probability of immune response. Similarly, first-order uniformity that reflects tumor homogeneity was associated with a higher probability of response.

As a first step toward clinical application of our model, we tested it on two independent samples of patients with urinary bladder and lung cancer. In these test cohorts, the radiomics signature identified patients who benefited from treatment, with 73% sensitivity and 55% specificity in the bladder cancer cohort and 73% sensitivity and 57% specificity in the lung cancer cohort. The moderately high sensitivity of this assay indicates a potential to better identify patients who may benefit from immune checkpoint inhibitors and in whom this treatment may be prioritized.

In this study, we showed that integrating clinical data (albumin and lymphocytes at baseline) improved performance compared with clinical-only and radiomics-only signatures (AUC, 0.74 vs 0.64 and 0.70, respectively).

To assess for a biologic basis of the radiomics signature, we explored its association with cytotoxic immunophenotyping by gene expression profiling as a marker of tumor immunogenicity (32,33). There was no statistically significant relationship between high CT-based radiomics score and enriched cytotoxic phenotype.

Few studies have been published on radiomics as a tool to assist in the medical treatment of patients with cancer undergoing immunotherapies. Sun et al (18) developed a CD8+ tumor infiltration radiomics signature. In line with our results, Sun et al demonstrated that tumor homogeneity was associated with high CD8+ tumor infiltration. Similarly, image acquisition parameters were considered for their radiomics signature development. Unfortunately, we could not correlate our signature with that of Sun et al because peritumoral radiomics features were included in their model, whereas we restricted our analysis to tumor features only because the periphery of tumors can contain artifacts (from contrast-enhanced vessels, fat, or air when the tumor is located at the organ edge).

With the advent of new tools for automatic or semiautomatic image segmentation and computational image analysis and quantification of radiomics signature scores, our signature could be incorporated into clinical trials and clinical practice in the near future. Whereas our data are reassuring regarding the biologic validity of our radiomics signature, further correlative studies in larger populations should now be performed in other tumor types including correlations with PD-L1 expression, microsatellite instability status, and tumor mutation burden, all of which are approved as predictive biomarkers for immune checkpoint inhibitor therapy (34).

Our study had some limitations. First, because of the observational and retrospective nature of the work, no standardization of image acquisition parameters was possible. Second, we developed a radiomics signature in a sample of multiple tumor types and validated in only two specific tumor types (bladder and lung cancer), which makes the training cohort more heterogeneous. Third, this predictive radiomics signature may be useful for anti–PD-1/PD-L1 patient selection but will require further testing in other cohorts as newer immunotherapies emerge. Last, our primary end point, clinical benefit, may not be used in pivotal trials, although we also identified an association between our signature and overall survival.

In conclusion, the CT-based radiomics signature developed in this study was associated with response to immune checkpoint inhibitors in patients with advanced solid tumors. The integration of multidimensional data including radiomics, clinical variables and genomic characterization may be key to optimize immune checkpoint inhibitor treatment selection and, ultimately, improve survival and quality of life in patients with cancer.

Acknowledgment: Guillermo Villacampa provided statistical advice for this manuscript.

Author contributions: Guarantors of integrity of entire study, M.L., A.G.R., M.V.R., J.L., R.M.B., R.P.L.; study concepts/study design or data acquisition or data analysis/interpretation, all authors; manuscript drafting or manuscript revision for important intellectual content, all authors; approval of final version of submitted manuscript, all authors; agrees to ensure any questions related to the work are appropriately resolved, all authors; literature research, M.L., M.V.R., I.M., J.M., J.R., E.M.C., A.O., J.S., M.E., J.T., R.D., E.G., R.P.L.; clinical studies, M.L., C.V., J.L., I.M., J.M.L., M.O.d.O., J.M., M.G., C.S., J.R., E.E., I.B., E.M.C., A.O., J.T., E.G.; experimental studies, M.L., A.G.R., C.V., M.V.R., I.M., R.M.B., A.O., R.F., P.N., J.S., J.T., R.P.L.; statistical analysis, M.L., A.G.R., G.V., I.M., A.O., D.G., C.R.P., J.S., J.T., R.D., R.P.L.; and manuscript editing, M.L., M.V.R., I.M., J.M.L., J.M., R.M.B., C.S., E.E., E.M.C., A.O., J.T., J.C., R.D., E.G., R.P.L.

Disclosures of Conflicts of Interest: **M.L.** disclosed no relevant relationships. **A.G.R.** disclosed no relevant relationships. **C.V.** disclosed no relevant relationships. **G.V.** Activities related to the present article: disclosed fees for participation in review activities from AstraZeneca and MSD. Activities not related to the present article: disclosed employment from SOLTI group. Other relationships: disclosed no relevant relationships. **M.V.R.** disclosed no relevant relationships. **J.L.** disclosed no relevant relationships. **I.M.** Activities related to the present article: disclosed no relevant relationships. Activities not related to the present article: disclosed ESMO fellowship in translational research. Other relationships: disclosed no relevant relationships. **J.M.L.** Activities related to the present article: disclosed no relevant relationships. Activities not related to the present article: disclosed consultancies from Bristol-Myers-Squibb, Novartis, Pierre Fabre, Roche; disclosed payment for lectures from Astellas, Bristol-Myers-Squibb, MSK, Novartis, Pierre Fabre, Pfizer, Roche; disclosed travel expenses from Bristol-Myers-Squibb, MSD, Novartis, Pierre Fabre, Pfizer, Roche, Ipsen. Other relationships: disclosed no relevant relationships. **M.O.d.O.** disclosed no relevant relationships. **C.H.** disclosed no relevant relationships. **J.M.** Activities related to the present article: disclosed no relevant relationships. Activities not related to the present article: disclosed consultancies from AstraZeneca, Roche, Amgen, Janssen, Clovis Oncology, MSD; grants/grants pending from AstraZeneca, Pfizer; payment for lectures from Astellas, AstraZeneca. Other relationships: disclosed no relevant relationships. **M.G.** Activities related to the present article: disclosed travel support from Roche, Astellas, Bayer. Activities not related to the present article: disclosed no relevant relationships. Other relationships: disclosed no relevant relationships. **R.M.B.** Activities related to the present article: disclosed no relevant relationships. Activities not related to the present article: disclosed employment from VHIO; grants from MSD; travel support from Roche, Sanofi, Aventis, MSD. Other relationships: disclosed no relevant relationships. **C.S.** disclosed no relevant relationships. **J.R.** Activities related to the present article: disclosed no relevant relationships. Activities not related to the present article: disclosed consultancies from Novartis, Eli Lilly, Orion Pharmaceuticals, Servier Pharmaceuticals, Peptomyc, Merck Sharp & Dohme, Kelun Pharmaceutical/Klus Pharma, Spectrum Pharmaceuticals Inc, Pfizer, Roche Pharmaceuticals, Ellipses Pharma, Certera, Bayer, Molecular Phartners, NovellusDX, Ionctura SA; disclosed grants/grants pending from Bayer, Novartis, Blueprint Pharmaceuticals, Spectrum Pharmaceuticals, Tocagen, Synphogen, BioAlta, Pfizer, GenMab, CytomX, Kelun-Biotech, Takeda-Millenium, GlaxoSmithKline, Ipsen; disclosed travel support from ESMO, Department of Defense, Merck Sharp & Dohme, Louisiana State University, Kelun Pharmaceutical/Klus Pharma, Huntsman Cancer Institute, Cancer Core Europe, Karolinska Cancer Institute, King Abdullah International Medical Research Center, Bayer, WIN Consortium, Jansen, Molecular Partners; disclosed other from European Journal of Cancer, VHIO/Ministero De Empleo Y Seguridad Social, Chinese University of Hong Kong, Solti, Elsevier, GlaxoSmithKline. Other relationships: disclosed no relevant relationships. **E.E.** Activities related to the present article: disclosed no relevant relationships. Activities not related to the present article: disclosed consultancies from Hoffman La Roche, Bristol Myers Squibb, Servier, Amgen, Merck Serono, Array Biopharma, Sanofi; honoraria from Array Biopharma, MSD, Abbvie, Amgen, GlaxoSmithKline, AstraZeneca, Merck Sharp and Dohme, Bristol Myers Squibb, Novartis, Boehringer Ingelheim, Hoffman La-Roche. Other relationships: disclosed no relevant relationships. **I.B.** Activities related to the present article: disclosed no relevant relationships. Activities not related to the present article: disclosed consultancies from MSD, Orion Pharma, Rakuten Aspyrian; expert testimony from Roche; grants/grants pending from MSD, BMS, Novartis, Astra Zeneca, Regeneron, GlaxoSmithKline, Kura, Pfizer, Orion Pharma, Merck Serono, Celgene, Incyte, Shattuck Lab, Janssen, Rakuten Aspyrian, VCN Biosciences; payment for lectures from BMS, Astra Zeneca, Merck Serono; travel support from Merck Serono, Astra Zeneca; and other from Instituto Salud Carlos III - Programa Rio Hortega Contract (grant CM15/00255). Other relationships: disclosed no relevant relationships. **E.M.C.** Activities related to the present article: disclosed consulting fees or honorarium from BMS, MSD, Novartis, Roche, Sanofi, Pierre-Fabre; disclosed travel support from BMS, MSD, Novartis. Activities not related to the present article: disclosed payment for expert testimony from BMS, Sanofi; disclosed payment for lectures from BMS, MSD, Sanofi, Roche, Pierre-Fabre. Other relationships: disclosed no relevant relationships. **A.O.** Activities related to the present article: disclosed no relevant relationships. Activities not related to the present article: disclosed no relevant relationships. Other relationships: disclosed advisory board service for Roche, AstraZeneca, PharmaMar, Clovis Oncology, Tesaro, Inmunogen

and Genmab; travel support from Roche, AstraZeneca, and PharmaMar; institutional financial interest from Abbvie Deutschland, Abililty Pharmaceuticals, Advaxis, Aeterna Zentaris, AMGEM, Aprea Therapeutics, Clovis Oncology, EISAI, F. Hoffmann – La Roche, Regeneron Pharmaceuticals, mmunogen, Merck, Sharp and Dohme de España, Millennium Pharmaceuticals, Pharma Mar, Tesaro, BMS, Bristrol Meyers Squibb. **R.F.** disclosed no relevant relationships. **P.N.** disclosed no relevant relationships. **D.G.** disclosed no relevant relationships. **C.R.P.** disclosed no relevant relationships. **J.S.** Activities related to the present article: disclosed ISCIII grant. Activities not related to the present article: disclosed board membership from Northern Biologics; consultancies from Mosaic Biomedicals, SLU; grants/grants pending from Hoffman La Roche, Ridgeline, Isarna Therapeutics, Mosaic Biomedicals, Fundación Científica De La Aecc; disclosed patents issued. Other relationships: disclosed no relevant relationships. **E.F.** Activities related to the present article: disclosed no relevant relationships. Activities not related to the present article: disclosed grants/grants pending from Fundacion Merck Salud, Merck Grant for Oncology Innovation; payment for lectures From Abbvie, Astra Zeneca, Blue Print Medicines, Boehringer Ingelheim, Bristol-Myers Squibb, Eli Lilly And Company, F. Hoffman -La Roche, Guardant Health, Janssen Biotech, Medscape, Merck Kgaa, Merck Sharp And Dohme, Novartis, Pfizer, Prime Oncology, Samsung, Takeda Oncology, Touchime. Other relationships: disclosed independent member of the board of directors from Grifols. **M.E.** disclosed no relevant relationships. **J.T.** Activities related to the present article: disclosed no relevant relationships. Activities not related to the present article: disclosed consultancies from Array Biopharma, AstraZeneca, Bayer, BeiGene, Boehringer Ingelheim, Chugai, Genentech, Inc., Genmab A/S, Halozyme, Imugene Limited, Inflection Biosciences Limited, Ipsen, Kura Oncology, Lilly, MSD, Menarini, Merck Serono, Merrimack, Merus, Molecular Partners, Novartis, Peptomyc, Pfizer, Pharmacyclics, ProteoDesign SL, Rafael Pharmaceuticals, F. Hoffmann-La Roche, Sanofi, SeaGen, Seattle Genetics, Servier, Symphogen, Taiho, VCN Biosciences, Biocartis, Foundation Medicine, HalioDX SAS, Roche Diagnostics. Other relationships: disclosed no relevant relationships. **J.C.** Activities related to the present article: disclosed no relevant relationships. Activities not related to the present article: disclosed board memberships from Bayer, Johnson & Johnson, Bristol-Myers Squibb Astellas Pharma, Pfizer, Sanofi, MSD Oncology, Roche, AstraZéneca; consultancy from Astellas; grants/grants pending from AB Science, Aragon Pharmaceuticals, Arog Pharmaceuticals, Astellas Pharma, Astrazeneca, Aveo Pharmaceuticals, Bayer, Blueprint Medicines, BN Immunotherapeutics, Boehringer Ingelheim España, Bristol-Myers Squibb International, Clovis Oncology, Cougar Biotechnology, Deciphera Pharmaceuticals, Exelixis, F. Hoffmann-La Roche, Genentech, Glaxosmithkline, Incyte Corporation, Janssen-Cilag International, Karyopharm Therapeutics, Laboratoires Leurquin Mediolanum, Lilly, Medimmune, Millennium Pharmaceuticals, Nanobiotix, Novartis Farmacéutica, Pfizer, SLU, Puma Biotechnology, Sanofi-Aventis, SFJ Pharma, Teva Pharma; payment for lectures from Bayer, Astellas, MSD; travel support from BMS, Roche, AstraZeneca. Other relationships: disclosed no relevant relationships. **R.D.** Activities related to the present article: disclosed no relevant relationships. Activities not related to the present article: disclosed consultancy for Roche; grants/grants pending for Roche, Ipsen, Amgen, Servier, Sanofi, Merck Sharp & Dohme, Boehringer Ingelheim. Other relationships: disclosed no relevant relationships. **E.G**. Activities related to the present article: disclosed no relevant relationships. Activities not related to the present article: disclosed consultancies for F.Hoffmann-La Roche, Ellipses Pharma, Neomed Therapeutics1 Inc, Boehringer Ingelheim, Janssen Global Services, Bristol-Mayers Squibb; travel support from Merck Sharp & Dohme, Glycotope, Menarini. Other relationships: disclosed no relevant relationships. **R.P.L.** disclosed no relevant relationships.

References

1. Long GV, Weber JS, Larkin J, et al. Nivolumab for patients with advanced melanoma treated beyond progression: analysis of 2 phase 3 clinical trials. JAMA Oncol 2017;3(11):1511–1519.
2. Postow MA, Chesney J, Pavlick AC, et al. Nivolumab and ipilimumab versus ipilimumab in untreated melanoma. N Engl J Med 2015;372(21):2006–2017 [Published correction appears in N Engl J Med 2018;379(22):2185.].
3. Ribas A, Puzanov I, Dummer R, et al. Pembrolizumab versus investigator-choice chemotherapy for ipilimumab-refractory melanoma (KEYNOTE-002): a randomised, controlled, phase 2 trial. Lancet Oncol 2015;16(8):908–918.
4. Bellmunt J, de Wit R, Vaughn DJ, et al. Pembrolizumab as second-line therapy for advanced urothelial carcinoma. N Engl J Med 2017;376(11):1015–1026.
5. Powles T, Durán I, van der Heijden MS, et al. Atezolizumab versus chemotherapy in patients with platinum-treated locally advanced or metastatic urothelial carcinoma (IMvigor211): a multicentre, open-label, phase 3 randomised controlled trial. Lancet 2018;391(10122):748–757 [Published correction appears in Lancet 2018;392(10156):1402.].
6. Motzer RJ, Escudier B, McDermott DF, et al. Nivolumab versus everolimus in advanced renal-cell carcinoma. N Engl J Med 2015;373(19):1803–1813.
7. Motzer RJ, Tannir NM, McDermott DF, et al. Nivolumab plus ipilimumab versus sunitinib in advanced renal-cell carcinoma. N Engl J Med 2018;378(14):1277–1290.
8. Brahmer J, Reckamp KL, Baas P, et al. Nivolumab versus docetaxel in advanced squamous-cell non-small-cell lung cancer. N Engl J Med 2015;373(2):123–135.
9. Borghaei H, Paz-Ares L, Horn L, et al. Nivolumab versus docetaxel in advanced nonsquamous non-small-cell lung cancer. N Engl J Med 2015;373(17):1627–1639.
10. Herbst RS, Baas P, Kim DW, et al. Pembrolizumab versus docetaxel for previously treated, PD-L1-positive, advanced non-small-cell lung cancer (KEYNOTE-010): a randomised controlled trial. Lancet 2016;387(10027):1540–1550.
11. Seymour L, Bogaerts J, Perrone A, et al. iRECIST: guidelines for response criteria for use in trials testing immunotherapeutics. Lancet Oncol 2017;18(3):e143–e152 [Published correction appears in Lancet Oncol 2019;20(5):e242.].
12. Nishino M, Hatabu H, Hodi FS. Imaging of cancer immunotherapy: current approaches and future directions. Radiology 2019;290(1):9–22.
13. Jardim DL, de Melo Gagliato D, Giles FJ, Kurzrock R. Analysis of drug development paradigms for immune checkpoint inhibitors. Clin Cancer Res 2018;24(8):1785–1794.
14. Tang J, Shalabi A, Hubbard-Lucey VM. Comprehensive analysis of the clinical immuno-oncology landscape. Ann Oncol 2018;29(1):84–91.
15. Buder-Bakhaya K, Hassel JC. Biomarkers for clinical benefit of immune checkpoint inhibitor treatment-a review from the melanoma perspective and beyond. Front Immunol 2018;9:1474.
16. Gibney GT, Weiner LM, Atkins MB. Predictive biomarkers for checkpoint inhibitor-based immunotherapy. Lancet Oncol 2016;17(12):e542–e551.
17. Lambin P, Leijenaar RTH, Deist TM, et al. Radiomics: the bridge between medical imaging and personalized medicine. Nat Rev Clin Oncol 2017;14(12):749–762.
18. Sun R, Limkin EJ, Vakalopoulou M, et al. A radiomics approach to assess tumour-infiltrating CD8 cells and response to anti-PD-1 or anti-PD-L1 immunotherapy: an imaging biomarker, retrospective multicohort study. Lancet Oncol 2018;19(9):1180–1191.
19. Aerts HJ, Velazquez ER, Leijenaar RT, et al. Decoding tumour phenotype by noninvasive imaging using a quantitative radiomics approach. Nat Commun 2014;5(1):4006.
20. Tang C, Hobbs B, Amer A, et al. Development of an immune-pathology informed radiomics model for non-small cell lung cancer. Sci Rep 2018;8(1):1922.
21. Trebeschi S, Drago SG, Birkbak NJ, et al. Predicting response to cancer immunotherapy using noninvasive radiomic biomarkers. Ann Oncol 2019;30(6):998–1004.
22. Gerlinger M, Rowan AJ, Horswell S, et al. Intratumor heterogeneity and branched evolution revealed by multiregion sequencing. N Engl J Med 2012;366(10):883–892 [Published correction appears in N Engl J Med 2012;367(10):976.].
23. Caswell DR, Swanton C. The role of tumour heterogeneity and clonal cooperativity in metastasis, immune evasion and clinical outcome. BMC Med 2017;15(1):133.
24. Fedorov A, Beichel R, Kalpathy-Cramer J, et al. 3D Slicer as an image computing platform for the Quantitative Imaging Network. Magn Reson Imaging 2012;30(9):1323–1341.
25. Parmar C, Barry JD, Hosny A, Quackenbush J, Aerts HJWL. Data analysis strategies in medical imaging. Clin Cancer Res 2018;24(15):3492–3499.
26. van Griethuysen JJM, Fedorov A, Parmar C, et al. Computational radiomics system to decode the radiographic phenotype. Cancer Res 2017;77(21):e104–e107.
27. Zwanenburg A, Vallières M, Abdalah MA, et al. The Image Biomarker Standardization Initiative: standardized quantitative radiomics for high-throughput image-based phenotyping. Radiology 2020;295(2):328–338.
28. Eisenhauer EA, Therasse P, Bogaerts J, et al. New response evaluation criteria in solid tumours: revised RECIST guideline (version 1.1). Eur J Cancer 2009;45(2):228–247.
29. Ohorodnyk P, Eisenhauer EA, Booth CM. Clinical benefit in oncology trials: is this a patient-centred or tumour-centred end-point? Eur J Cancer 2009;45(13):2249–2252.
30. Pascual-García M, Bonfill-Teixidor E, Planas-Rigol E, et al. LIF regulates CXCL9 in tumor-associated macrophages and prevents $CD8^+$ T cell tumor-infiltration impairing anti-PD1 therapy. Nat Commun 2019;10(1):2416.

31. Balagurunathan Y, Gu Y, Wang H, et al. Reproducibility and prognosis of quantitative features extracted from CT images. Transl Oncol 2014;7(1):72–87.
32. Charoentong P, Finotello F, Angelova M, et al. Pan-cancer immunogenomic analyses reveal genotype-immunophenotype relationships and predictors of response to checkpoint blockade. Cell Rep 2017;18(1):248–262.
33. Angelova M, Charoentong P, Hackl H, et al. Characterization of the immunophenotypes and antigenomes of colorectal cancers reveals distinct tumor escape mechanisms and novel targets for immunotherapy. Genome Biol 2015;16:64.
34. Tray N, Weber JS, Adams S. Predictive biomarkers for checkpoint immunotherapy: current status and challenges for clinical application. Cancer Immunol Res 2018;6(10):1122–1128.